Dual-Mode Conductor-Loaded Cavity Filters[1]

Chi Wang, Kawthar A. Zaki, *Fellow, IEEE,* and Ali E. Atia, *Fellow, IEEE*

***Abstract*— A new class of dual-mode filters consisting of cylindrical-waveguide cavities loaded with perfect conducting cylindrical disks is presented. Resonant frequencies, fields, and the unloaded Q of the resonator are rigorously analyzed by mode-matching techniques. A complete set of data for filter design is given. The results show that the resonator has high unloaded Q and good spurious performance. The accuracy of the computed results are confirmed by comparison with the experimental data. An eight-pole elliptic-function filter for PCS applications was designed, constructed, and tested; excellent frequency response of the filter with wide spurious-free performance was obtained, which verifies the theory.**

I. Introduction

DUAL-MODE filters have many advantages in applications requiring small size and mass for high-quality narrow or medium bandwidth filters, because of their lower loss, small volume, and elliptic-function response. Since their introduction in the early 1970's [1], they have been widely used in satellite communications as well as other areas. Tremendous progress has been achieved on further miniaturization of the dual-mode filters in the past two decades. The use of dielectric-loaded resonators greatly improves the in-band performance, size, and thermal stability of the dual-mode filters [2]–[8].

Although dual-mode dielectric-loaded resonator filters have many advantages, one of their major disadvantages is their inferior out-of-band spurious characteristics. Dielectric resonator filters usually need an additional low-pass filter, which will increase the insertion loss and complexity of the filter [5]. Significant effort has been spent on improving the spurious performance of dielectric-loaded resonator filters, especially dual-mode filters [6], [10], [11].

While dielectric materials of excellent characteristics have been developed with relative dielectric constant in the range of 20–38, higher dielectric-constant materials tend to have poorer properties (high losses, less temperature stability, etc.). Higher dielectric constants are desirable to reduce the size of the filters. If one thinks of increasing the relative dielectric constant of the dielectric resonator to approach infinity $(\epsilon_r \rightarrow \infty)$, the resonator approaches a perfect conductor. Thus, if the dielectric resonator in a dual-mode filter is replaced by a perfect electric conductor, significant miniaturization can be achieved, and high-quality filters can be realized. Additionally, in applications of using superconductors, filters with extremely low insertion loss can be achieved. The resonator operating in HE_{11} mode will have much higher unloaded Q and easier realization of elliptic-function response than that of the metallic-ring resonator in a cavity operating in quasi-TEM mode.

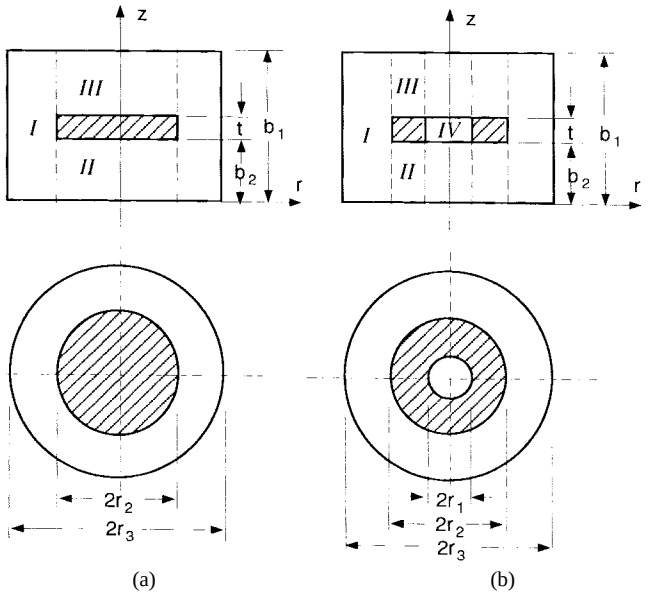

Fig. 1. Configuration of the cylindrical conductor-loaded resonator. (a) Solid conductor-loaded resonator and (b) ring conductor-loaded resonator.

In this paper, a new class of dual-mode filters consisting of cylindrical-waveguide cavities loaded with perfect conducting cylindrical (solid or ring) resonators is introduced. Rigorous mode-matching techniques are used to analyze and synthesize the new type of resonators. Resonant frequencies and field distributions of the resonant modes in the cavities are obtained. The unloaded Q of the resonant mode is analytically computed from the eigenfunctions and field coefficients in each region. The calculated resonant frequencies are compared with the measured results and shown to be in good agreement, which confirms the correctness and accuracy of the numerical results. The computer simulation shows that the HE_{11} mode of the conductor-loaded resonator has high unloaded Q and much better spurious performance than a dielectric-loaded resonator. Mode charts and Q charts provide a complete set of data for the filter design.

An eight-pole elliptic-function filter for personal-communication system (PCS) applications was designed, constructed, and tested. Excellent frequency response with low insertion loss and superior spurious-free performance was obtained.

II. Analysis

The configurations of the resonators under consideration are shown in Fig. 1. The resonator consists of a cylindrical

Manuscript received January 14, 1997; revised April 25, 1997.

C. Wang and K. A. Zaki are with the Department of Electrical Engineering, University of Maryland, College Park, MD 20742 USA.

A. E. Atia is with CTA Inc., Rockville, MD 20852 USA.

Publisher Item Identifier S 0018-9480(97)05380-5.

[1]Patent assigned to the University of Maryland.

conducting disk with radius r_2, and thickness t, coaxially surrounded by a cylindrical enclosure of radius r_3 and total height b_1. Fig. 1(a) shows the solid-type resonator, and Fig. 1(b) shows the ring-type resonator with a hole of radius r_1 at the center of the disk.

The analysis of the structures is performed using the mode-matching techniques, in which the structures are partitioned into several regions in accordance with the spatial discontinuity boundaries, as shown in Fig. 1. The solid-type resonator can be considered as a special case of the ring type. The transverse electromagnetic (EM) fields in each region are expressed as linear combinations of the eigenmode fields as [9]

$$\begin{aligned}\vec{E}_t^p(\rho,\phi,z) =& \sum_j^{N_p^e}\{C_j^{pe}\mathcal{B}_{CEj}^{pe}(\rho)+D_j^{pe}\mathcal{B}_{DEj}^{pe}(\rho)\}\\ &\times\vec{e}_{tj}^{pe}(\rho,\phi,z)\\ &+\sum_j^{N_p^h}\{C_j^{ph}\mathcal{B}_{CEj}^{ph}(\rho)+D_j^{ph}\mathcal{B}_{DEj}^{ph}(\rho)\}\\ &\times\vec{e}_{tj}^{ph}(\rho,\phi,z) \qquad (1a)\\ \vec{H}_t^p(\rho,\phi,z) =& \sum_j^{N_p^e}\{C_j^{pe}\mathcal{B}_{CHj}^{pe}(\rho)+D_j^{pe}\mathcal{B}_{DHj}^{pe}(\rho)\}\\ &\times\vec{h}_{tj}^{pe}(\rho,\phi,z)\\ &+\sum_j^{N_p^h}\{C_j^{ph}\mathcal{B}_{CHj}^{ph}(\rho)+D_j^{ph}\mathcal{B}_{DHj}^{ph}(\rho)\}\\ &\times\vec{h}_{tj}^{ph}(\rho,\phi,z) \qquad (1b)\\ \xi_j^{pq^2} =& k_0{}^2\epsilon_r^p-k_j^{pq2}, \qquad p=I,II,III, \text{ or } IV,\\ & q=e,h \qquad (1c)\end{aligned}$$

where ξ_j^{pq} represent the wavenumbers of the TE and TM modes in the corresponding region, respectively; $\mathcal{B}_j^{pq}$ are first- and second-kind Bessel functions J_n, Y_n, or associated Bessel functions I_n, K_n and their derivatives depending on the value of $\xi_j^{pq^2}$, $\vec{e}_{tj}^{pq}$, $\vec{h}_{tj}^{pq}$ are the transverse eigenfields of TE mode ($q=h$) or TM mode ($q=e$) of two parallel-plane waveguides bounded in the z-direction, and are given in the Appendix, C_j^{pe}, D_j^{pq} are the field coefficients in each region. $D_j^{pq}=0$ in the region where $\rho=0$ is included. D_j^{Iq} is related to C_j^{Iq} by

$$D_j^{Ie} = -\frac{J_n(\xi_j^{Ie}r_3)}{Y_n(\xi_j^{Ie}r_3)}C_j^{Ie} \qquad (2a)$$

$$D_j^{Ih} = -\frac{J_n'(\xi_j^{Ih}r_3)}{Y_n'(\xi_j^{Ih}r_3)}C_j^{Ih}. \qquad (2b)$$

For the ring-type resonator, the boundary conditions at the interface of regions II, III, and IV require the tangential electric and magnetic fields to be continuous at $\rho=r_1$, i.e.,

$$\begin{aligned}&\vec{E}_t^{IV}(\rho=r_1,\phi,z)\\ &\quad=\begin{cases}\vec{E}_t^{II}(\rho=r_1,\phi,z), & 0\le z\le b_2\\ 0, & b_2\le z\le b_2+t\\ \vec{E}_t^{III}(\rho=r_1,\phi,z), & b_2+t\le z\le b_1\end{cases} \qquad (3a)\\ &\vec{H}_t^{IV}(\rho=r_1,\phi,z)\\ &\quad=\begin{cases}\vec{H}_t^{II}(\rho=r_1,\phi,z), & 0\le z\le b_2\\ \vec{J}_s\times\hat{n}, & b_2\le z\le b_2+t.\\ \vec{H}_t^{III}(\rho=r_1,\phi,z), & b_2+t\le z\le b_1\end{cases} \qquad (3b)\end{aligned}$$

By taking the proper inner products, and using the orthogonal properties of the eigenfunctions, one has

$$\begin{aligned}&[\langle\vec{e}^{IV},\vec{h}^{IV}\rangle][\mathcal{B}_{CE}^{IV}][C^{IV}]\\ &\quad=[\langle\vec{e}^{II+III},\vec{h}^{IV}\rangle]\\ &\qquad\times\left\{[\mathcal{B}_{CE}^{II+III}]\begin{bmatrix}C^{II}\\C^{III}\end{bmatrix}+[\mathcal{B}_{DE}^{II+III}]\begin{bmatrix}D^{II}\\D^{III}\end{bmatrix}\right\} \qquad (4a)\\ &\qquad\times[\langle\vec{e}^{II+III},\vec{h}^{IV}\rangle]^T[\mathcal{B}_{CH}^{IV}][C^{IV}]\\ &\quad=[\langle\vec{e}^{II+III},\vec{h}^{II+III}\rangle]\\ &\qquad\times\left\{[\mathcal{B}_{CH}^{II+III}]\begin{bmatrix}C^{II}\\C^{III}\end{bmatrix}+[\mathcal{B}_{DH}^{II+III}]\begin{bmatrix}D^{II}\\D^{III}\end{bmatrix}\right\} \qquad (4b)\end{aligned}$$

with

$$\langle\vec{e}^{p_1},\vec{h}^{p_2}\rangle=\int_{S^p}\vec{e}^{p_1}\times\vec{h}^{p_2}\cdot\vec{\rho}\,d\phi\,dz. \qquad (5)$$

After some matrix manipulations, a matrix relating the field coefficients D_j^q to C_j^q of region II and III can be obtained

$$\begin{bmatrix}D^{II}\\D^{III}\end{bmatrix}=[T_{CD}^{II+III}]\begin{bmatrix}C^{II}\\C^{III}\end{bmatrix}. \qquad (6)$$

$[T_{CD}^{II+III}]$ has dimensions $N_{23}\times N_{23}$, $N_{23}=N_{II}^e+N_{II}^h+N_{III}^e+N_{III}^h$. All the elements of $[T_{CD}^{II+III}]$ are zero for the solid-type resonator.

Similarly, by applying the boundary condition at $\rho=r_2$, taking the inner product, and substituting $[T^{CD}]$ into the continuity equation, a matrix relating the field coefficients of region I can be obtained as follows:

$$[M_C^I][C^I]+[M_D^I][D^I]=0. \qquad (7)$$

$[M_C^I]$ and $[M_D^I]$ are matrices of size $N_1\times N_1$, where $N_1=N_I^e+N_I^h$ is the total number of eigenmodes used in region I.

From the boundary condition of the eigenmodes in the resonator at $\rho=r_3$, the characteristic equation for the resonant frequency of the resonator can finally be obtained. The determinant of the equation must be zero for nontrivial solutions

$$\det[X]_{N_1\times N_1}=0 \qquad (8a)$$

$$[X]=[M_C^I]+[M_D^I][T_{CD}^I]. \qquad (8b)$$

Solving the equation will give the resonant-frequency and field-expansion coefficients in region I, while the field coefficients in the other regions are obtained from the boundary-condition equation. The fields of the resonant mode in each region are readily computed by the superposition of the eigenmodes fields.

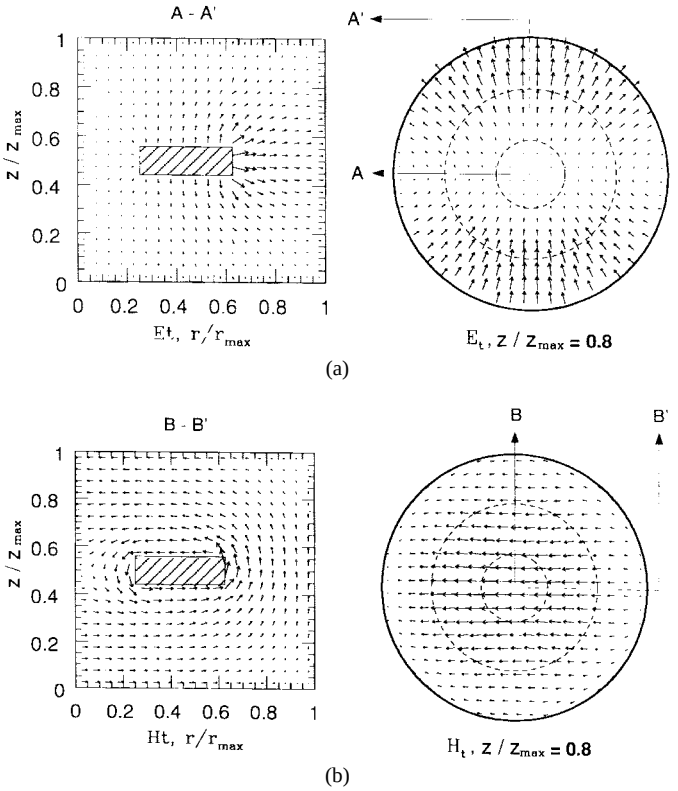

Fig. 2. Typical HE_{11}-mode field distributions of the conductor-loaded resonator. (a) Electric-field distribution and (b) magnetic-field distribution.

The unloaded Q of the resonator is determined by computing the stored energy and the conductor loss of both inner conductor and enclosure as

$$Q_0 = \omega_o \frac{W_0}{P_c} \tag{9a}$$

$$W_0 = \frac{1}{2}\int_V \mu_o |H|^2\, dv = \frac{1}{2}\mu_o \int_V \sum_p \left(\sum_j^{N^e, N^h} |H_j^{pe} + H_j^{ph}|^2 \right) dv \tag{9b}$$

$$P_c = \frac{1}{2}\oint_S R_s |H_t|^2\, ds = \frac{1}{2}\oint_S \sum_p R_s \left(\sum_j^{N^e, N^h} |H_{tj}^{pe} + H_{tj}^{ph}|^2 \right) ds. \tag{9c}$$

Where H is the magnetic field in the cavity, H_t is the tangential magnetic field at the surface of the conductor, and R_S is the surface resistance of the conductor. Since the magnetic fields are expressed in terms of the linear superposition of the mode fields, all the integrations in the equations can be carried out analytically. Using the orthogonal properties of the eigenmodes, the unloaded Q of the resonator can be computed efficiently.

III. Results

Computer programs have been developed to perform the analysis described above. Converging results can be obtained when the number of TE and TM eigenmodes is larger than 12 in region I. The number of modes used in other regions are taken as the ratio of the region's height to region I's height, times the number of modes in region I. A comparison of the calculated resonant frequencies of both solid- and ring-type resonators with the measured results is shown in Table I. Good agreement between numerical and experimental results confirms the correctness and accuracy of the computer programs. Fig. 2 shows the typical electric- and magnetic-field distributions of the HE_{11} mode of the conductor-loaded resonator in the r–z and r–ϕ planes. The electric and magnetic fields of the HE_{11} mode are orthogonal to each other, and they are very similar to the fields of the dielectric-loaded resonator. A degenerate HE_{11} mode exists, possessing the same resonant frequency, but with its field distributions rotated by 90° relative to the first mode. The field distributions show the realizability of the dual-mode filter. The continuity of the fields at the boundary of each region and their behavior on the conducting surface, once again, proves the correctness of the results.

TABLE I
Comparison of the Computed and Measured Resonant Frequencies (GHz) of a Conductor-Loaded Resonator with $b_1 = 1.9''$, $r_3 = 1.6''$, $t = 0.222''$

	SOLID $r_1 = 0$, $r_2 = 1.201$"		RING $r_1 = 0.9$", $r_2 = 1.051$"	
Mode	Computed	Measured	Computed	Measured
HE_{11}	1.940	1.936	1.883	1.879
TM_{01}	2.733	2.721	2.793	2.781
HE_{21}	3.322	3.317	3.507	3.501
TM_{02}	3.668	3.657	4.133	4.117
HE_{12}	4.378	4.355	4.277	4.262
HE_{31}	4.674	4.665	4.989	4.978
HE_{13}	5.060	5.037	4.395	4.373

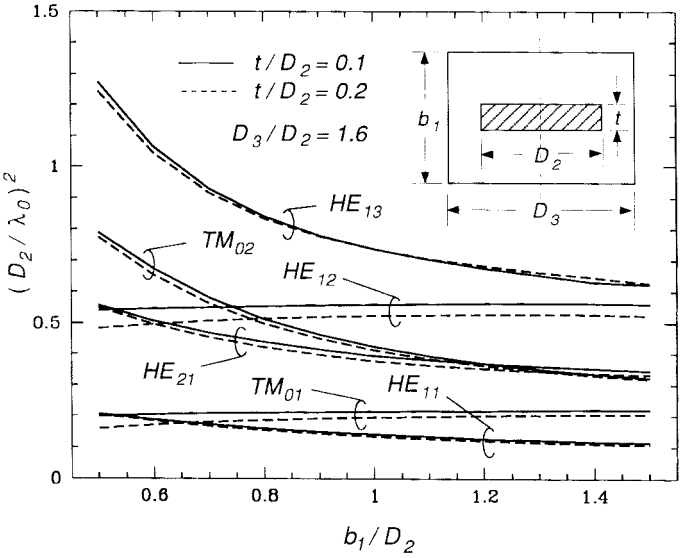

Fig. 3. Mode chart of the conductor-loaded resonator with b_1/D_2 as variable.

The mode charts have been computed to aid in the resonator design. Fig. 3 shows the dependence of the resonant frequencies on the height of the enclosure. It is shown that the resonant frequencies of the HE_{21}, TM_{02}, and HE_{13} modes are quite sensitive to the height, while the resonant frequencies of HE_{11}, TM_{01}, and HE_{12} are relatively stable. The mode chart

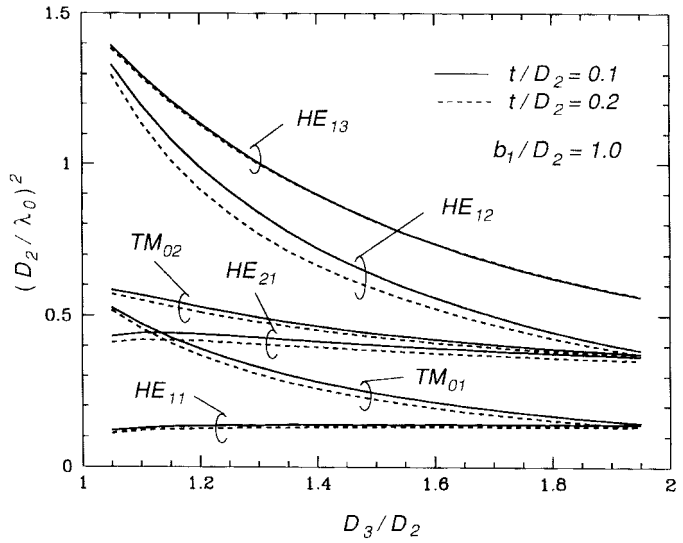

Fig. 4. Mode chart of the conductor-loaded resonator with D_3/D_2 as variable.

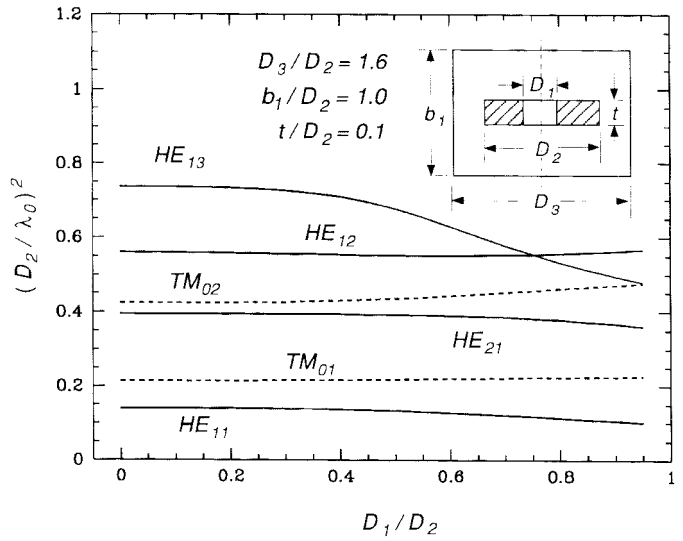

Fig. 5. The effect of the hole on the resonant frequency of the ring-type resonator.

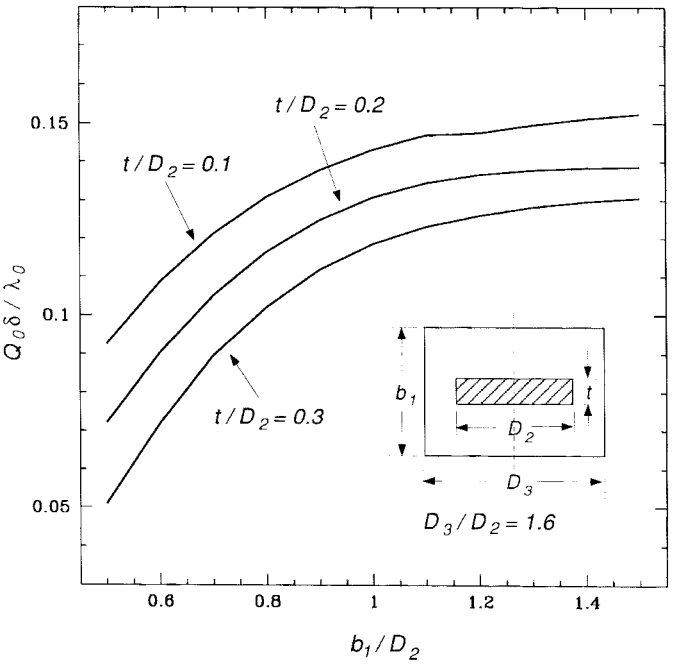

Fig. 6. Normalized unloaded Q of the resonator versus the b_1/D_2.

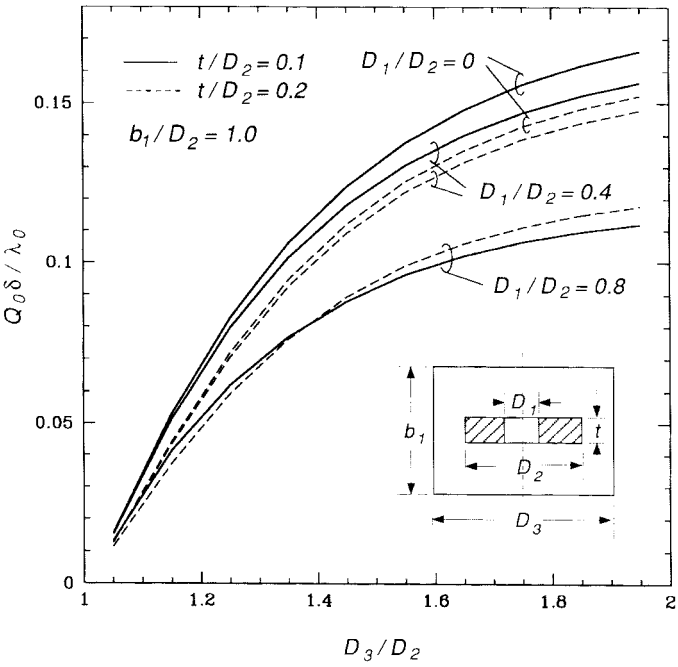

Fig. 7. Normalized unloaded Q of the resonator versus the D_3/D_2.

with the diameter of the enclosure as variable is presented in Fig. 4. All the modes move closer to the HE_{11} mode as the diameter of the enclosure increases, and the mode separation becomes worse. The two mode charts indicate an important property of the resonator, i.e., the resonant frequency of the HE_{11} mode is nearly independent of the dimension of the enclosure when the space between the inner conductor and the enclosure is large enough. If the inner conductor is made of temperature-constant material, the resonator will have very good temperature stability.

Fig. 5 shows how the resonant frequencies of the ring resonator vary versus the diameter of the hole. It is clear that the resonant frequencies of the resonator are very insensitive to the hole when the hole is not very large.

Fig. 6 presents the computed normalized unloaded Q of the conductor-loaded resonator having different thickness of the inner conductor versus the height of the enclosure. Fig. 7 shows the normalized unloaded Q of the resonators of both solid and ring types versus the diameter of the enclosure. Fig. 6 indicates that thicker inner conductor yields less unloaded Q, and Fig. 7 shows that larger hole also reduces unloaded Q. Both figures show that the unloaded Q of the resonator is very sensitive to the space between the inner conductor and the enclosure. Large losses result if top, bottom, or sidewall of the enclosure are close to the inner conductor. When $b_1/D_2 \geq 1.0$, $D_3/D_2 \geq 1.6$, the unloaded Q of the resonator tends to be insensitive to the size of the enclosure.

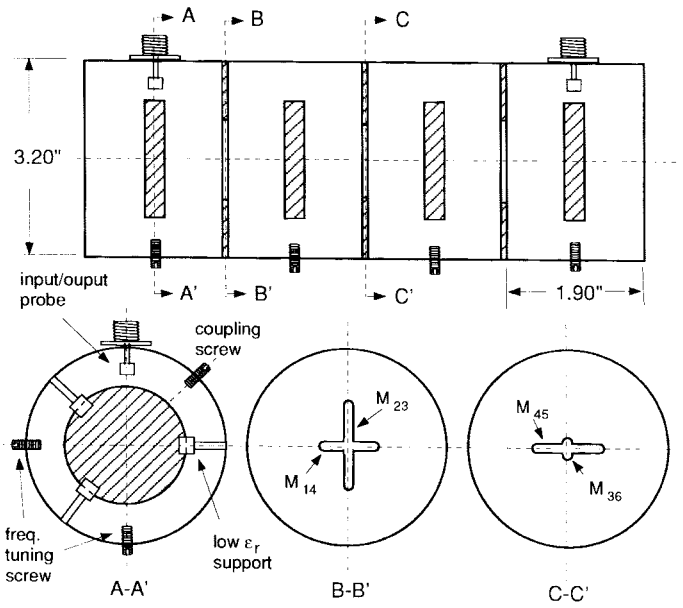

Fig. 8. Configuration of the eight-pole elliptic-function filter.

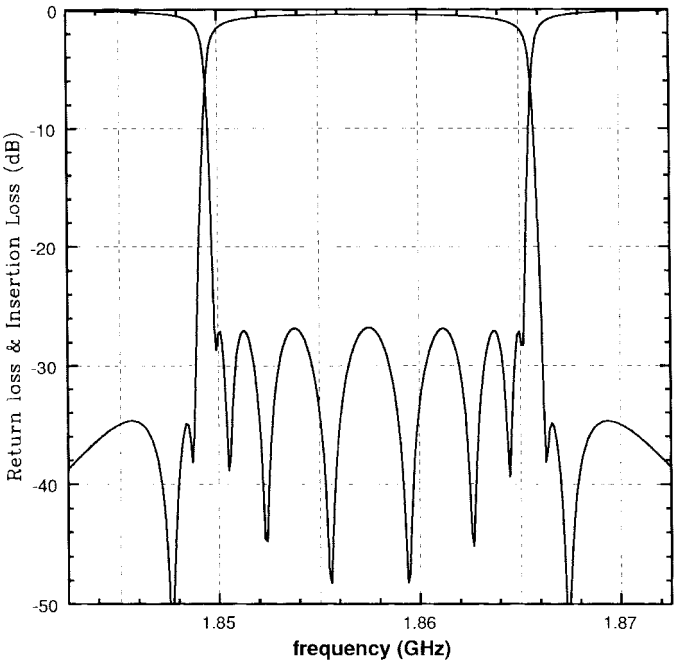

Fig. 9. Theoretical frequency responses of the eight-pole filter.

IV. Filter Realization

From the previous analysis, it is shown that the thickness of the inner conductor should be kept small and the enclosure should be large enough to achieve high unloaded Q. On the other hand, too large an enclosure will decrease the mode separation. The unloaded Q of the resonator is determined from the loss requirement of the filter. The dimensions of the resonator can be determined from the mode charts. The coupling matrix of the filter can be obtained from the given specifications by a synthesis procedure [1], and the iris dimensions are synthesized using small aperture-coupling theory [12]–[14].

An eight-pole elliptic-function filter for PCS base-station application with center frequency of 1.8575 GHz, and bandwidth of 15.5 MHz was designed, constructed, and tested. The input/output (I/O) resistances and coupling matrix elements of the filter are $R_1 = R_2 = 1.2101$, $M_{12} = M_{78} = 0.8153$, $M_{23} = M_{67} = 0.8465$, $M_{34} = M_{56} = 0.4292$, $M_{45} = 0.5408$, $M_{14} = M_{58} = -0.4119$, $M_{36} = -0.0109$. The dimension of the designed cavity is $r_3 = 1.6''$, $b_1 = 1.9''$ with theoretical unloaded Q of 9500 (silver-plated). Fig. 8 shows the configuration of the eight-pole filter. Tuning screws oriented at 0° and 90° to the normal field polarization in each cavity are used for fine tuning the resonant frequency of the resonators. A coupling screw oriented 45° to the normal field polarization is used to couple the dual degenerate modes. Couplings between resonators of different cavities are achieved by irises. The inner conductors are supported by the low dielectric constant dielectric clips at the side of the conductors as shown in Fig. 8. The theoretical frequency response of the filter is shown in Fig. 9.

Fig. 10 shows the measured frequency responses of the filter. The insertion loss is 0.81 dB, which corresponds to average unloaded Q of about 6000. If the center metallic loading disk is made from a superconductor, and the outer cylinder is made from copper, the theoretical unloaded Q would be about 30 000 and the corresponding midband insertion loss would be about 0.14 dB at 77 K.

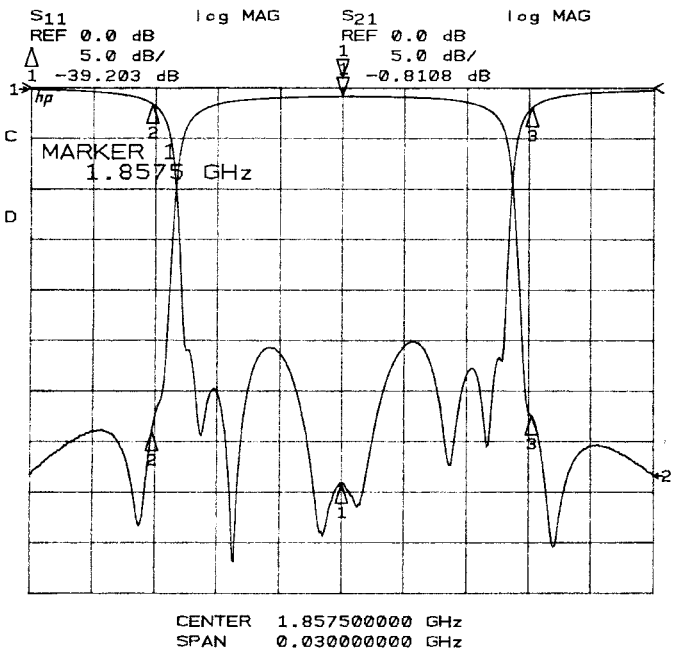

Fig. 10. Measured frequency responses of the eight-pole dual-mode elliptic-function filter.

Fig. 11 gives the wide-band frequency response of the eight-pole filter. It is seen that the TM_{01} mode response is not excited. The first higher order mode spurious response occurs at 3.59 GHz, which is approximately twice the filter's center frequency. This is a much larger separation of the spurious frequency than can be achieved by empty waveguide cavities or dielectric-loaded resonators.

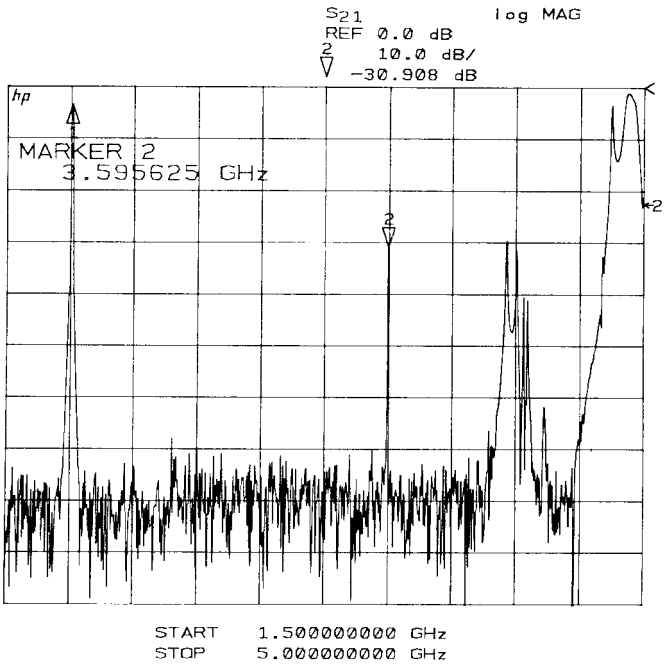

Fig. 11. Wide-band frequency response of the eight-pole dual-mode elliptic-function filter.

V. Conclusions

The introduction of a conductor resonator-loaded cylindrical enclosure using the hybrid HE_{11} dual mode for the realization of high-quality filters has been presented. Rigorous mode-matching techniques are used to analyze and synthesize the new type of resonators. The accuracy of the computed results are confirmed by experiment. A complete set of mode charts and Q data are provided for filter design. An eight-pole elliptic-function filter for PCS applications is designed, constructed, and tested, with excellent frequency responses. The spurious performance of the filter is superior to both empty and dielectric-loaded cavity filters. The conductor-loaded dual-mode filter is an excellent candidate for superconductor realization in wireless PCS base stations, as well as other applications. The new filter configuration has potential for excellent performance and lower production cost than alternative realizations.

Appendix

This appendix gives the expressions for the function $\mathcal{B}(\rho)$ and the transverse eigenfields of two parallel-plane waveguides $\vec{e}_{tj}^{pq}$ and $\vec{h}_{tj}^{pq}$.

A. Expressions for $\mathcal{B}(\rho)$

$$\mathcal{B}_{CEj}^{pe}(\rho)=\begin{cases}J_n(|\xi_j^{pe}|\rho), & \xi_j^{pe^2}\geq 0\\ I_n(|\xi_j^{pe}|\rho), & \xi_j^{pe^2}\leq 0\end{cases} \tag{A1}$$

$$\mathcal{B}_{CEj}^{ph}(\rho)=\begin{cases}J_n'(|\xi_j^{ph}|\rho), & \xi_j^{ph^2}\geq 0\\ I_n'(|\xi_j^{ph}|\rho), & \xi_j^{ph^2}\leq 0\end{cases} \tag{A2}$$

$$\mathcal{B}_{DEj}^{pe}(\rho)=\begin{cases}Y_n(|\xi_j^{pe}|\rho), & \xi_j^{pe^2}\geq 0\\ K_n(|\xi_j^{pe}|\rho), & \xi_j^{pe^2}\leq 0\end{cases} \tag{A3}$$

$$\mathcal{B}_{DEj}^{ph}(\rho)=\begin{cases}Y_n'(|\xi_j^{ph}|\rho), & \xi_j^{ph^2}\geq 0\\ K_n'(|\xi_j^{ph}|\rho), & \xi_j^{ph^2}\leq 0\end{cases} \tag{A4}$$

$$\mathcal{B}_{CHj}^{pe}(\rho)=\begin{cases}J_n'(|\xi_j^{pe}|\rho), & \xi_j^{pe^2}\geq 0\\ I_n'(|\xi_j^{pe}|\rho), & \xi_j^{pe^2}\leq 0\end{cases} \tag{A5}$$

$$\mathcal{B}_{CHj}^{ph}(\rho)=\begin{cases}J_n(|\xi_j^{ph}|\rho), & \xi_j^{ph^2}\geq 0\\ I_n(|\xi_j^{ph}|\rho), & \xi_j^{ph^2}\leq 0\end{cases} \tag{A6}$$

$$\mathcal{B}_{DHj}^{pe}(\rho)=\begin{cases}Y_n'(|\xi_j^{pe}|\rho), & \xi_j^{pe^2}\geq 0\\ K_n'(|\xi_j^{pe}|\rho), & \xi_j^{pe^2}\leq 0\end{cases} \tag{A7}$$

$$\mathcal{B}_{DHj}^{ph}(\rho)=\begin{cases}Y_n(|\xi_j^{ph}|\rho), & \xi_j^{ph^2}\geq 0\\ K_n(|\xi_j^{ph}|\rho), & \xi_j^{ph^2}\leq 0.\end{cases} \tag{A8}$$

B. Expressions for the Eigenfunction $\vec{e}_{tj}^{pq}$ and $\vec{h}_{tj}^{pq}$

$$\vec{e}_{tj}^{pe}(\rho,\phi,z)=\hat{z}\begin{Bmatrix}\sin(n\phi)\\ \cos(n\phi)\end{Bmatrix}\cos(k_j^{pe}z')-\hat{\phi}\frac{1}{\xi_j^{pe^2}}\frac{n}{\rho}\begin{Bmatrix}\cos(n\phi)\\ -\sin(n\phi)\end{Bmatrix}\times k_j^{pe}\sin(k_j^{pe}z') \tag{A9}$$

$$\vec{e}_{tj}^{ph}(\rho,\phi,z)=\hat{\phi}\frac{1}{\xi_j^{ph^2}}\{\cos(n\phi)-\sin(n\phi)\}\times\sin(k_j^{ph}z') \tag{A10}$$

$$j\omega\mu_o\vec{h}_{tj}^{pe}(\rho,\phi,z)=\hat{\phi}\frac{k_o^2\epsilon_r^p}{\xi_j^{pe^2}}\begin{Bmatrix}\sin(n\phi)\\ \cos(n\phi)\end{Bmatrix}\times\cos(k_j^{pe}z') \tag{A11}$$

$$j\omega\mu_o\vec{h}_{tj}^{ph}(\rho,\phi,z)=\hat{z}\begin{Bmatrix}\cos(n\phi)\\ -\sin(n\phi)\end{Bmatrix}\sin(k_j^{ph}z')-\hat{\phi}\frac{1}{\xi_j^{ph^2}}\frac{n}{\rho}\begin{Bmatrix}\sin(n\phi)\\ \cos(n\phi)\end{Bmatrix}\times k_j^{ph}\cos(k_j^{ph}z') \tag{A12}$$

$$k_j^{pq}=\frac{j\pi}{d_p},\qquad p=I,\,II,\,III,\ \text{or}\ IV;\ q=e,\,h \tag{A13}$$

where d_p is the height of region p, $z'=z-b_2-t$ for region III, and $z'=z$ for the rest of the regions, and n is the azimuthal variation of the desired mode.

Acknowledgment

The authors wish to thank all the reviewers who gave numerous thorough, helpful, and constructive comments and suggestions for improvements.

References

[1] A. E. Atia and A. E. Williams, "Narrow-bandpass waveguide filters," *IEEE Trans. Microwave Theory Tech.*, vol. MTT-20, pp. 258–265, Apr. 1972.

[2] S. B. Cohn, "Microwave bandpass filters containing high-Q dielectric resonators," *IEEE Trans. Microwave Theory Tech.*, vol. MTT-16, pp. 218–227, Apr. 1968.
[3] W. H. Harrison, "A miniature high-Q bandpass filter employing dielectric resonators," *IEEE Trans. Microwave Theory Tech.*, vol. MTT-16, pp. 210–218, Apr. 1968.
[4] S. J. Fiedziuszko, "Dual-mode dielectric resonator loaded cavity filters," *IEEE Trans. Microwave Theory Tech.*, vol. MTT-30, pp. 1311–1316, Sept. 1982.
[5] ———, "Practical aspects and limitations of dual mode dielectric resonator filters," in *IEEE Int. Microwave Theory Symp. Dig.*, St. Louis, MO, June 1985, pp. 353–356.
[6] Y. Kobayashi and M. Minegishi, "Precise design of a bandpass filter using high-Q dielectric ring resonators," *IEEE Trans. Microwave Theory Tech.*, vol. MTT-35, pp. 1156–1160, Dec. 1987.
[7] Y. Kobayashi and K. Kubo, "Canonical bandpass filters using dual-mode dielectric resonators," in *IEEE Int. Microwave Theory Symp. Dig.*, Las Vegas, NV, June 1987, pp. 137–140.
[8] K. A. Zaki, C. Chen, and A. E. Atia, "Canonical and longitudinal dual-mode dielectric resonator filters without iris, *IEEE Trans. Microwave Theory Tech.*, vol. MTT-35, pp. 1130–1135, Dec. 1987.
[9] S.-W. Chen and K. A. Zaki, "Dielectric ring resonators loaded in waveguide and on substrate," *IEEE Trans. Microwave Theory Tech.*, vol. 39, pp. 2069–2076, Dec. 1991.
[10] R. V. Snyder, "Dielectric resonator filter with wide stop-bands," *IEEE Trans. Microwave Theory Tech.*, vol. 40, pp. 2100–2102, Nov. 1992.
[11] J.-F. Liang, K. A. Zaki, and A. E. Atia, "Mixed mode dielectric resonators filters," *IEEE Trans. Microwave Theory Tech.*, vol. 42, pp. 2449–2454, Dec. 1994.
[12] R. Levy, "Improved single and multiaperture waveguide coupling theory, including explanation of mutual interactions," *IEEE Trans. Microwave Theory Tech.*, vol. MTT-28, pp. 331–338, Apr. 1980.
[13] H.-W. Yao, J.-F. Liang, and K. A. Zaki, "Accuracy of coupling computations and its application," in *IEEE MTT-S Int. Microwave Symp.*, San Diego, CA, May 1994, pp. 723–726.
[14] G. L. Matthaei, L. Young, and E. M. T. Jones, *Microwave Filters, Impedance-Matching Networks, and Coupling Structure.* New York: McGraw-Hill, 1984.

Chi Wang received the B.S. and M.S. degrees, both in electrical engineering, from Beijing Institute of Technology, Beijing, China, in 1983 and 1986, respectively. He is currently working toward the Ph.D. degree in electrical engineering at the University of Maryland, College Park.

From 1986 to 1989, he was an Electrical Engineer at North China Vehicle Research Institute, Beijing, China, where he was engaged in developing a vehicle's electrical system and its auto test system. From 1990 to 1992, he was involved in the study of home satellite receivers and audio and video systems at Beijing XYE Electronics, Inc. He spent one year as Research Associate at Beijing Institute of Technology, working on modeling of antennas and resonators, using the finite-difference time-domain method. Since 1994, he has held the Graduate Research Assistantship with Microwave Research Group, University of Maryland, College Park, where he has done research on analysis, modeling, and design of dielectric and conductor-loaded resonators and filters, coaxial resonator filters, HTS and LTCC filters, ultra-high Q sapphire resonators, ridge waveguide, and T-junctions. Between 1994 and 1995, he also held the position of Graduate Teaching Assistant. His current research interests are in the areas of modeling and computer-aided design of RF/microwave components, integrated circuits, and optoelectronics.

Kawthar A. Zaki (SM'85–F'91) received the B.S. degree with honors from Ain Shams University, Cairo, Egypt, in 1962, and the M.S. and Ph.D. degrees from the University of California, Berkeley, in 1966 and 1969, respectively, all in electrical engineering.

From 1962 to 1964, she was a Lecturer in the Department of Electrical Engineering, Ain Shams University. From 1965 to 1969, she held the position of Research Assistant in the Electronic Research Laboratory, University of California at Berkeley. She joined the Electrical Engineering Department, University of Maryland, College Park, in 1970, where she is presently Professor of electrical engineering. Her research interests are in the areas of electromagnetics, microwave circuits, optimization, computer-aided design, and optically controlled microwave and millimeter-wave devices.

Ali E. Atia (S'67–M'69–SM'78–F'87) received the B.S. degree from Ain Shams University, Cairo, Egypt, in 1962, and the M.S. and Ph.D. degrees from the University of California at Berkeley, in 1966 and 1969, respectively, all in electrical engineering.

Prior to joining COMSAT in 1969, he held various research and teaching positions at Ain Shams University and the University of California at Berkeley. As a Senior Scientist in the Microwave Laboratory at COMSAT Laboratories, he has made original contributions to satellite transponders and antenna technologies, most notably the development of the dual-mode microwave filters technology. He has also made significant contributions to several satellite programs, including INTELSAT IV-A, V, V-A, VI, and ARABSAT. He was responsible for the design, implementation, qualification, and testing of major subsystems in COMSAT's NASA ATS-F propagation experiment and COMSTAR Ka-band beacon experiment. As Senior Director in COMSAT Systems Division, he was responsible for communications systems design, integration, implementation, and testing under contracts with various government and commercial customers. From 1989 to 1994, he served as Vice President and Chief Engineer for COMSAT Technology Services. In 1994, he joined CTA Inc., in Rockville, MD, as President of its wholly owned subsidiary CTA International.

Dr. Atia is an Associate Fellow of the AIAA and a Member of Sigma Xi. He was a joint recipient of the 1997 Microwave Pioneer Award.